# Two and Three-dimensional Through-Bond Homonuclear-Heteronuclear Correlation Experiments for Quadrupolar Nuclei in Solid-State NMR Applied to 27Al-O-31P-O-27Al networks

M. Deschamps, D. Massiot

# Two and Three-dimensional Through-Bond Homonuclear-Heteronuclear Correlation Experiments for Quadrupolar Nuclei in Solid-State NMR Applied to $^{27}$Al-O-$^{31}$P-O-$^{27}$Al networks

Michaël Deschamps*, Dominique Massiot,

CRMHT-CNRS, 1D Avenue de la Recherche Scientifique,

45071 ORLEANS cedex 2, France

* michael.deschamps@cnrs-orleans.fr

Keywords: 3D, J-coupling, quadrupolar nuclei, aluminium, phosphate

To be submitted to Concepts in Magnetic Resonance

23/01/2008

## Abstract

Through-bond correlation experiments can be realised in solids between spins of type X, separated by four chemical bonds, in X-O-Y-O-X molecular motives, provided a scalar coupling (J) between X and Y exists. In the 2D-Homonuclear-Heteronuclear Single Quantum Correlation (H-HSQC) experiment presented here, the central transitions of quadrupolar $^{27}$Al spins can be correlated via the scalar coupling $J^2$ between $^{27}$Al (X) and $^{31}$P (Y) in materials featuring Al-O-P-O-Al motives. A 3D homonuclear/heteronuclear correlation experiment can also be performed, providing the correlation map characterizing the two $^{27}$Al and the $^{31}$P NMR signatures of $^{27}$Al-O-$^{31}$P-O-$^{27}$Al chemically bonded molecular motifs.

## Introduction

3D J-mediated correlation experiments have been introduced a long time ago in liquid state NMR experiments *(1)*. They characterize triplets of atoms which are connected together, and, as such, are very powerful to characterize the network of chemical bonds in a solution or in a solid-state sample as well. High resolution solid-state experiments can make efficient use of the scalar coupling (*J*) in MAS experiments on organic and inorganic solids *(2, 3)*, despite the heterogeneous line broadening mechanisms that usually mask the direct spectral expression of the scalar couplings, although benefiting from the increased sensitivity and resolution obtained at high MAS spinning rates and high magnetic fields *(4)*. Dynamic Angle Spinning (DAS) also enhance the resolution for quadrupolar nuclei *(5)*. Among mesoporous materials made from $AlPO_4$, $AlPO_4$-14 has already been studied by X-ray crystallography *(6, 7)* and NMR *(7-9)* and will be used for demonstration. Its structure is well known and similar to those of zeolithes, however, the framework is entirely built up with $AlO_x$ (x = 4, 5 or 6) and $PO_4$ polyhedrons. Four, five and six-fold coordination states are observed for the Al atoms and Al are connected together by either bridging oxygen atoms or O-P-O chains (Figure 1). Four different sites can be distinguished for Al and also for P atoms *(7)*. $Al_1$ is five fold coordinated trigonal-bipyramidal (bonded to 4 -O-P-$(O\text{-}Al)_4$ and 1 -O-Al), $Al_2$ and $Al_3$ are four fold coordinated tetrahedra (bonded to 4 -O-P-$(O\text{-}Al)_4$) and $Al_4$ is a six fold coordinated octahedra (bonded to 4 -O-P-$(O\text{-}Al)_4$ and 2 -O-Al).

In contrast with liquid state experiments in which the short relaxation times observed for quadrupolar nuclei often precludes their proper manipulation by NMR, several 2D dipolar mediated or J-mediated homonuclear and heteronuclear correlation methods have been introduced for solid-state experiments involving one or two quadrupolar nuclei like $^{27}Al$ (S=5/2)

*(7-14)*, $^{71}$Ga (S=3/2) *(15)* or $^{27}$Al and $^{17}$O (S=5/2) *(16)*. The efficiency of $^{27}$Al / $^{31}$P (S=1/2) experiments benefits from their 100% natural abundance and their good receptivity, with an increased sensitivity at high field thanks to a lower second order quadrupolar broadening for the $^{27}$Al spin *(17)*. Moreover, the magnetization of the $^{27}$Al central transition (which is only affected by the second-order quadrupolar broadening) can be efficiently enhanced by transferring the populations from the satellite transitions to the central transition using methods like DFS or RAPT *(18-19)*.

In solid-state, the 2D or 3D HHSQC experiments allow to characterize structural motifs involving three different spins (2 $^{27}$Al and 1 $^{31}$P in a Al-O-P-O-Al linkage) in a 3 dimensional experiment, correlating the 1D spectra of the three bonded nuclei (2×$^{27}$Al and 1×$^{31}$P). The 2D HHSQC only gives the homonuclear {$^{27}$Al, $^{27}$Al} two dimensional correlation map selectively for the Al-O-P-O-Al motifs. Because the scalar coupling $J_2$(X-O-Y) is used, the 2D/3D H-HSQC spectra allow identification of molecular entities extending over 4 chemical bonds and typically over 0.4 to 0.5 nm in size. Despite its low sensitivity, this experiment provides a unique way for obtaining unambiguously this type of information.

## Theory

The 2D/3D homonuclear/heteronuclear correlation experiment (3D H-HSQC) makes use of the sole scalar coupling (*J*) to transfer the magnetization (see Figure 2). This results in a robust and rather simple pulse sequence that only involves manipulation of the spin system with soft π/2 and π pulses, which ensures manipulation of the $^{27}$Al central transition as a fictitious spin 1/2. The transfer occurs from the first aluminium atom to the neighbouring phosphorus and then to a second aluminium through the isotropic part $J_2$(Al-O-P) of the scalar coupling in an Al-O-P-O-Al group and provides experimental evidence for through-bond correlations between the $Al_1$, P and

$Al_2$ nuclei in $Al_1$-O-P-O-$Al_2$ motives with spectral identification of the resonances of these three nuclei in the different projections. Because the experiment uses the scalar coupling it does not require any reintroduction of interaction averaged out by MAS and it undergoes no limitation with the spinning rate which is usually required to achieve better resolution. It only requires long enough transverse relaxation times $T_2$' (typically 15 ms in our case) and a sufficient sensitivity for the acquisition of the 2D or 3D datasets within a reasonable experimental time.

The experiment consists in two INEPT transfers separated by a constant time period achieving the magnetization transfer and containing the $^{31}P$ encoding time $t_2$. The first INEPT transfer leads to the creation of a density operator proportional to $2Al^1_{z,CT}P_y$ (where the aluminium central transition is described as a fictitious spin 1/2) after an evolution under the scalar coupling during a delay $2\tau$ (1/4J). The second constant time echo period ($2\ \tau_2$) allows for the conversion of $Al^1_{z,CT}P_y$ into $Al^2_{z,CT}P_y$, which gives rise to a negative cross-peak in the 2D or 3D H-HSQC spectrum. The positive diagonal signal corresponds to the remaining $Al^1_{z,CT}P_y$ term. This transfer depends upon n', the number of $^{27}Al$ spins coupled to the $^{31}P$ nucleus. The functions describing the intensities of the diagonal signal ($Al^1_{z,CT}P_y$) and of the cross-peaks (stemming from the conversion of $Al^1_{z,CT}P_y$ into $Al^2_{z,CT}P_y$) are given below. Equations (1), (2) and (3) correspond to n'=2, 3 and 4, respectively, with an initial density operator $\sigma(\tau_2=0) = 2Al^1_{z,CT}P_y$ :

$$I\left(Al^1_z P_y\right) = -1/2\left[1+\cos 4\pi J\tau_2\right] \text{ and } I\left(Al^2_z P_y\right) = -1/2\left[-1+\cos 4\pi J\tau_2\right] \quad (1)$$

$$I\left(Al^1_z P_y\right) = 1/4\left[\cos 6\pi J\tau_2 + 3\cos 2\pi J\tau_2\right] \text{ and } I\left(Al^2_z P_y\right) = 1/4\left[\cos 6\pi J\tau_2 - \cos 2\pi J\tau_2\right] \quad (2)$$

$$I\left(Al^1_z P_y\right) = 1/8\left[3+4\cos 4\pi J\tau_2 + \cos 8\pi J\tau_2\right] \text{ and } I\left(Al^2_z P_y\right) = 1/8\left[-1+\cos 8\pi J\tau_2\right] \quad (3)$$

The two expressions in Eq. (3) are plotted in Figure 3 as a function of $\tau_2$ in $1/J$ units. The $^{31}P$ chemical shift evolves during the delay $t_2$, and the $^{31}P$ scalar couplings to the neighbouring $^{27}Al$ spins evolve in a constant time manner during $2\tau_2$ (see Figure 2).

## Discussion

For the 2D experiment, the dataset is Fourier transformed against the two evolution times and the resulting spectrum is shown in Figure 4. The different spectral contributions are indicated on the spectrum. The third evolution time in the 3D experiment allows to separate the ($Al_x$, $Al_y$) cross-peaks with respect to the $^{31}P$ chemical shift in the $Al_x$-O-$P_z$-O-$Al_y$ motif. In the 3D experiment, the resulting three dimensional hypercomplex dataset is Fourier transformed against the three evolution times and Figure 5B-D shows one $^{27}Al/^{27}Al$ plane (with the *x* and *y* axis corresponding to the direct and indirect $^{27}Al$ dimensions) extracted from the 3D matrix (as shown in Figure 5A) and corresponding to the phosphorus chemical shift of the $P_2$ site $\delta(^{31}P) = -8.03$ ppm. Hence, the extracted 2D spectrum will eventually feature the residual negative diagonal peaks of some $Al_x$-O-$P_2$ group and the positive cross-peaks of any $Al_x$-O-$P_2$-O-$Al_y$ groups. Three different strips along the $^{31}P$ axis, perpendicular to the $^{27}Al/^{27}Al$ plane and intersecting with it in the cross (indicating an $Al_x$,$Al_y$ peak), are superimposed on the 2D spectrum. If $Al_x$ and $Al_y$ are also connected via O-$P_n$-O, the $P_n$ peak will appear in the superimposed strip. In (B), the cross is located on the *negative* (hence diagonal) $Al_1$, $Al_1$ peak in the plane corresponding to $P_2$, indicating that a diagonal peak is observed for the triplet $Al_1$, $P_2$, $Al_1$, and the corresponding strip (intersecting with the Al, Al plane in ($\delta(Al_1)$,$\delta(Al_1)$) as indicated by the cross) along the $^{31}P$ axis features three additional peaks corresponding to $P_1$, $P_3$ and $P_4$ indicating that similar $Al_1$, $Al_1$ diagonal correlations are observed in the planes corresponding to the chemical shifts of $P_1$, $P_3$ and $P_4$ respectively. Hence $Al_1$ is never connected to another $Al_1$ via an O-P-O group, because only *negative* diagonal peaks have been observed, and $Al_1$ is bonded to $P_1$, $P_2$, $P_3$ and $P_4$. In (C), the cross is located on the $Al_2$, $Al_4$ cross-peak, indicating that $Al_2$ and $Al_4$ are connected via an O-$P_2$-O linkage (because the extracted 2D spectrum corresponds to $P_2$). Two peaks are observed in the

strip for the chemical shifts of $P_2$ and $P_4$, hence the cross-peaks between $Al_2$ and $Al_4$ are observed in the two following groups: $Al_2$-O-$P_2$-O-$Al_4$ (observable in the plane $\delta(P_2)$ which is represented in the figure) and $Al_2$-O-$P_4$-O-$Al_4$ (observable in the plane $\delta(P_4)$, not represented here). This complies with the known connectivity table (Table 1) which has been established previously *(8, 9)*. A similar conclusion can be inferred from Figure 5D, where $P_1$, $P_3$ and $P_4$ connect to both the $Al_1$ and $Al_3$ atoms.

## Experimental

Weak (selective, i.e. $\nu_1 \approx 4$ kHz) pulses have been used on the $^{27}Al$ central transition (described as a fictitious spin 1/2), which is prepared by enhancement from the satellite transitions by DFS *(17)* transfer using a 2 ms pulse with$\nu_1 \approx 8$ kHz (RAPT *(18)* can also be used).

Two Z-filters (300 rotor periods or 21 ms) have been used in the pulse sequence to simplify the phase cycle and suppress unwanted contributions of undetermined origin which were observed without the Z-filter. Unfortunately such long Z-filter delays are approaching the order of the $T_1$ value, and some signal is lost during the Z-filter. A cleaning $B_0$ field gradient instead would have the desired effect but was unfortunately unavailable on our MAS probes.

The times $\tau$ and $\tau_2$ were set to 40 rotor periods (2.86 ms) and 120 rotor periods (8.57 ms) respectively, and the $J^2(^{27}Al,^{31}P)$ values (unobservable in this case) are estimated to be in the 10-30Hz range. To optimize $\tau$ and $\tau_2$, $\tau_2$ was first set to zero and $\tau$ has been optimized to get the largest positive signal. Then $\tau_2$ is increased and optimized to obtain the largest negative signal, as shown in Figure 3. Quantification of the peak intensities requires similar transfer efficiencies: Different $T_2$ and J-coupling values would lead to different transfer efficiencies, precluding a proper interpretation of the peak intensities.

The MAS speed was set to 14 kHz and a magnetic field $B_0$ =17.6 T (750 Mhz $^{1}$H Larmor frequency with $^{27}$Al and $^{31}$P Larmor frequency equal to 194.5 and 303.7 MHz respectively) was used. 1024 scans, 16 dummy scans, 40 increments in F1 and F2, 512 points in F3 and a recycling delay of 250 ms have been used for an overall experimental time of 6 days and 13h on a 750MHz wide bore Bruker spectrometer. The optimum recycling delay, which depends upon the relaxation behaviour of the central and satellite transitions (because DFS is used), was determined by comparing the signal obtained in the permanent regime for various recycling delays, and 250 ms was considered as optimal, as it allowed a 95% recovery.

Indirect quadrature detection was achieved using the States method, whereas DQD was used during acquisition. A spectral width of 14 kHz was used in the three dimensions, corresponding exactly to the MAS spinning speed, in order to sum any remaining spinning sidebands *(21)*. The data have been processed with nmrPipe *(20)*, the spectrum is phased in order to have negative diagonal peaks and positive cross-peaks, and an exponential line broadening of 200 Hz has been applied in the three dimensions (the natural linewidth in the $^{31}$P dimension –without $^{1}$H and $^{27}$Al decoupling- is about 200 Hz, in the $^{27}$Al dimension, second order quadrupolar broadening is larger than the exponential line broadening factor).

## Conclusions

2D and 3D experiments correlating $Al_1$, P, $Al_2$ triplets in $Al_1$-O-P-O-$Al_2$ motives are feasible and confirm the connectivity graph of the Al/P network of a complex material such as $AlPO_4$-14. The significantly longer experimental time required for the 3D experiment (nearly 6 ½ days), as compared to the 2D Al, Al H-HSQC (1 day), is the price to be paid for the complete edition of connected $Al_x$-O-P-O-$Al_y$ motives. However, future hardware improvements such as higher

magnetic fields, faster MAS rate, the use of magnetic field gradients which will supersede Z-filters (especially in this experiment) and the eventual inclusion of MQMAS and/or $^{1}H$ decoupling and $^{27}Al$ satellite transitions refocusing during $t_1$ might increase the S/N ratio and the available resolution. The principle of this 3D H-HSQC could be extended to any system of three or more coupled spins and applied to many inorganic materials. It provides a detailed map of the coupled network, and a full characterization of chemically bonded molecular motives. When this information remains of little use for crystalline compounds of known structure, recent results show that it becomes decisive information for the characterization of structural motifs at the nanometer scale in amorphous solids or glasses *(16)*.

## Acknowledgments

We acknowledge financial support from CNRS UPR4212, FR2950, MIAT and Région Centre and we are grateful to Pr. P.J. Grandinetti, Drs. F. Fayon and V. Montouillout for stimulating discussions.

## References

(1) Cavanagh J, Fairbrother WJ, Palmer III AG, Skelton NJ. Protein NMR spectroscopy: principles and practice: Academic Press (San Diego); 1996.

(2) Sakellariou D, Emsley L. Through-Bond Experiments in Solids: The Encyclopedia of NMR, D.M. Grant and R.K. Harris (Eds.), J. Wiley and Sons: London; 2002.

(3) Massiot D, Fayon F, Alonso B, Trebosc J, Amoureux JP. Chemical bonding differences evidenced from J coupling in solid state NMR experiments involving quadrupolar nuclei. J Magn Reson 2005; 164:165.

(4) Gan Z, Gor'kov P, Cross TA, Samoson A, Massiot D. Seeking Higher Resolution and Sensitivity for NMR of Quadrupolar nuclei at ultrahigh magnetic fields. J Am Chem Soc 2002; 124:5634-5635.

(5) Grandinetti PJ. Dynamic-Angle Spinning and Applications. Encyclopedia of NMR 1995, 1768-1776.

(6) Helliwell M, Kaucic V, Cheetham GMT, Harding MM, Kariuki BM, Rizkallah PJ. Structure determination from small crystals of two aluminophosphates CrAPO-14 and SAPO-43. Acta Crystallogr 1993; B49:413.

(7) Fyfe CA, Meyer zu Altenschildesche H, Wong-Moon KC, Grondey H, Chezeau JM. 1D and 2D solid state NMR investigations of the framework structure of As-synthesized AlPO4-14. Solid State NMR 1997; 9:97-106.

(8) Delevoye L, Fernandez C, Morais CM, Amoureux JP, Montouillout V, Rocha J. Solid State NMR 2002 ; 22 :501-512.

(9) Wiench JW, Pruski M. Probing through bond connectivities with MQMAS NMR. Solid State NMR 2004; 26:51-55.

(10) Van Eck ERH, Veeman WS. Solid-state 2D heteronuclear $^{27}$Al-$^{31}$P correlation NMR spectroscopy of aluminophosphate VPI-5. J Am Chem Soc 1993; 115:1168-1169.

(11) Eden M, Grinshtein J, Frydman L. High resolution 3D exchange NMR spectroscopy and the mapping of connectivities between half-integer quadrupolar nuclei. J Am Chem Soc 2002; 124: 9708-9709; Eden M, Annersten H, Zazzi A. Pulse-assisted homonuclear dipolar recoupling of half-integer quadrupolar spins in magic-angle spinning NMR. Chem Phys Lett 2005; 410:24-30.

(12) Mali G, Fink G, Taulelle F. Double-quantum homonuclear correlation magic angle sample spinning nuclear magnetic resonance spectroscopy of dipolar-coupled quadrupolar nuclei. J Chem Phys 2004; 120:2835-2845.

(13) Deschamps M, Fayon F, Montouillout V, Massiot D. Through-bond homonuclear correlation experiments in Solid-state NMR applied to quadrupolar nuclei in Al-O-P-O-Al chains. Chem Comm 2006:1924-1925.

(14) Deschamps M, Massiot D. Three-dimensional Through-Bond Homonuclear-Heteronuclear Correlation Experiments for Quadrupolar Nuclei in Solid-State NMR applied to 27Al-O-31P-O-27Al networks. J Magn Reson 2006; 184:13-19.

(15) Montouillout V, Morais CM, Douy A, Fayon F, Massiot D. Towards a better description of gallo-phosphate materials in solid state NMR: 1D and 2D correlation studies. Magn Reson Chem (in press).

(16) Iuga D, Morais C, Gan Z, Neuville DR, Cormier L, Massiot D. NMR Heteronuclear Correlation between Quadrupolar Nuclei in Solids. J Am Chem Soc 2005; 127:11540-11541.

(17) Gan Z, Gor'kov P, Cross TA, Samoson A, Massiot D. Seeking Higher Resolution and Sensitivity for NMR of Quadrupolar nuclei at ultrahigh magnetic fields. J Am Chem Soc 2002; 124:5634-5635.

(18) Kentgens APM, Verhagen R. Advantages of double frequency sweep in static, MAS and MQMAS NMR of spin I=3/2 nuclei. Chem Phys Lett 1999; 300:435.

(19) Kwak HT, Prasad S, Clark T, Grandinetti PJ. Enhancing Sensitivity of Quadrupolar Nuclei in Solid-State NMR with Multiple Rotor Assisted Population Transfers. Solid State NMR 2003; 24:71-77.

(20) Delaglio F, Grzesiek S, Vuister GW, Zhu G, Pfeifer J, Bax A. NMRPipe: multidimensional spectral processing system based on UNIX pipes. J Biomol NMR 1995; 6:277-293.

(21) Massiot D. Sensitivity and lineshape improvements of MQ-MAS by rotor synchronized data acquisition. J Magn Reson A 1996; 122:240-244.

Figure legends

**Figure 1** Five schemes of the molecular motives involved are shown below in the $^{27}Al/^{31}P$ case, featuring: a) $Al^{IV}$, b) $Al^{V}$, c) $Al^{VI}$, d) Al-O-P-O-Al and e) Al-O-Al.

**Figure 2** Pulse sequence for: A) the 2D ($t_1$ incremented) and B) the 3D ($t_1$ and $t_2$ incremented) H-HSQC experiment. In C) the molecular motif which is edited, along with the necessary scalar couplings are represented. The $2\tau_2$ delay is a constant time period allowing for the magnetization transfer from the $Al_1$ spin to the $Al_2$ spin. $^{27}Al_1$ and $^{31}P$ chemical shift evolutions occur during the $t_1$ and $t_2$ delays respectively. Two Z-filters (300 rotor periods or 21 ms) have been used to suppress unwanted contributions. $\tau$ and $\tau_2$ were set to 40 rotor periods (2.86 ms) and 120 rotor periods (8.57 ms) respectively with a MAS speed of 14 kHz and $B_0$ =17.63 T (750 Mhz $^1H$ Larmor frequency). $\Phi_1 = \{0°, 180°\}$, $\Phi_2 = \{0°, 0°, 180°, 180°\}$and $\Phi_{rec} = \{0°, 180°, 180°, 0°\}$.

**Figure 3** Plots of the intensities of the diagonal ($2Al^1_{z,CT}P_y$) and cross-peak ($2Al^2_{z,CT}P_y$) and their sum (overall signal) as a function of $\tau_2$ in 1/J units. The optimum transfer is obtained for the largest negative overall signal (sum of the two contributions).

**Figure 4** H-HSQC spectrum of an $AlPO_4$-14 sample, featuring the Al-Al pairs giving rise to negative cross-peaks (in black) and the positive diagonal signals (in red). The spectrum was obtained in the experimental conditions mentioned in the Figure 2 caption. The pulse sequence was run using the following parameters: the recycling delay $d_1$ was set to 250ms, the $\tau$ period for the INEPT transfer was set to 40 rotor periods $\tau_r$ (optimized for the best overall signal-to-noise

ratio, as the different $^{27}$Al-$^{31}$P pairs feature distinct scalar couplings and dephasing times), the $\tau_2$ period was set to $120\tau_r$ (in order to maximize the negative cross peaks intensities), and a Z-filter of $300\tau_r$ was used on a 750MHz wide bore Bruker spectrometer. 16 dummy scans and 1152 scans were acquired for each of the 128 $t_1$ increments and exponential broadening (LB=100Hz) was applied in both dimensions.

**Figure 5** A 2D plane (as shown in (A)) is extracted from the 3D $^{27}$Al,$^{31}$P,$^{27}$Al H-HSQC, corresponding to the phosphorus chemical shift $\delta(^{31}P)$= –8.03 ppm (corresponding to $P_2$) and is displayed three times in (B), (C) and (D). Three different strips or slices along the $^{31}$P axis have been extracted, in the manner shown in (A) and are shown in (B), (C) and (D), respectively. In (B), (C) and (D), the respective intersections of the strip with the $^{27}$Al/$^{27}$Al plane are indicated by a cross, as shown in the 3D scheme. 1024 scans, 40 increments in F1 and F2, 512 points in F3 and a recycling delay of 250 ms have been used for an overall experimental time of 6 days and 13h on a 750MHz wide bore Bruker spectrometer. The data have been processed with nmrPipe *(19)*.

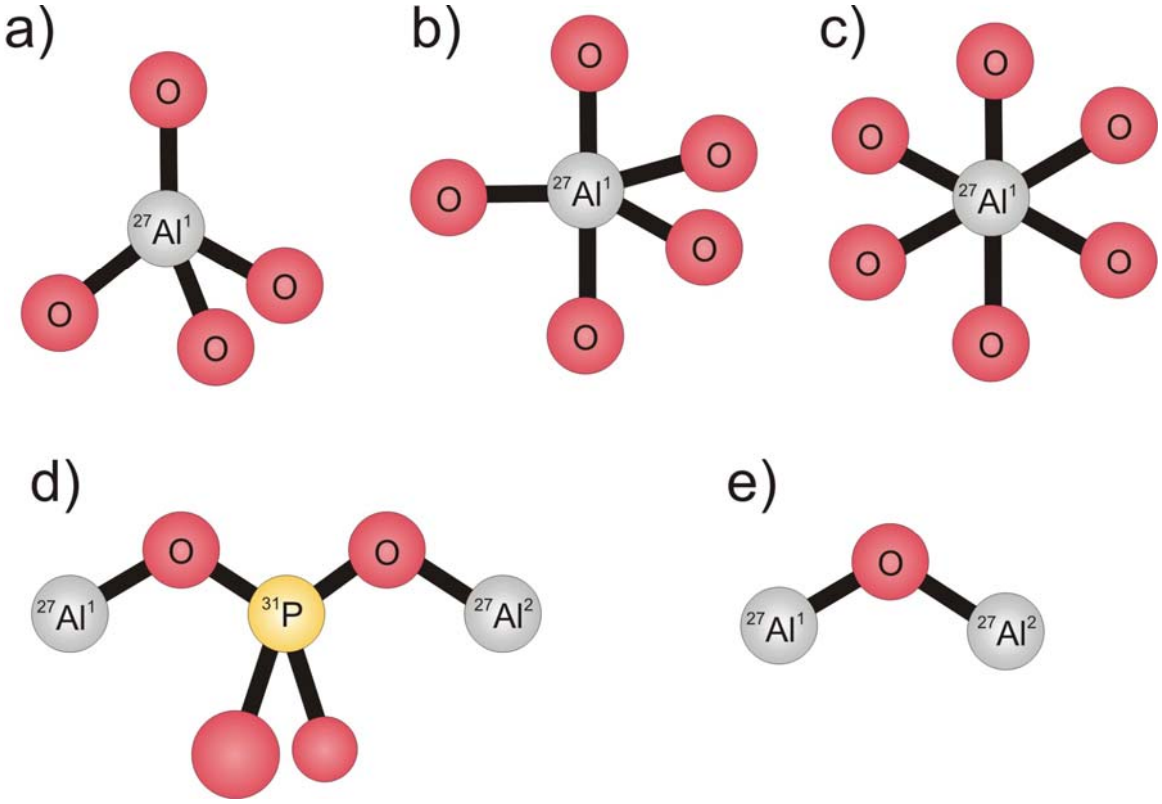
a)
O
$^{27}Al^{1}$
O
O
O
b)
O
O
$^{27}Al^{1}$
O
O
O
c)
O
O
O
$^{27}Al^{1}$
O
O
O
d)
O
O
$^{27}Al^{1}$
$^{31}P$
$^{27}Al^{2}$
e)
O
$^{27}Al^{1}$
$^{27}Al^{2}$

Figure 1

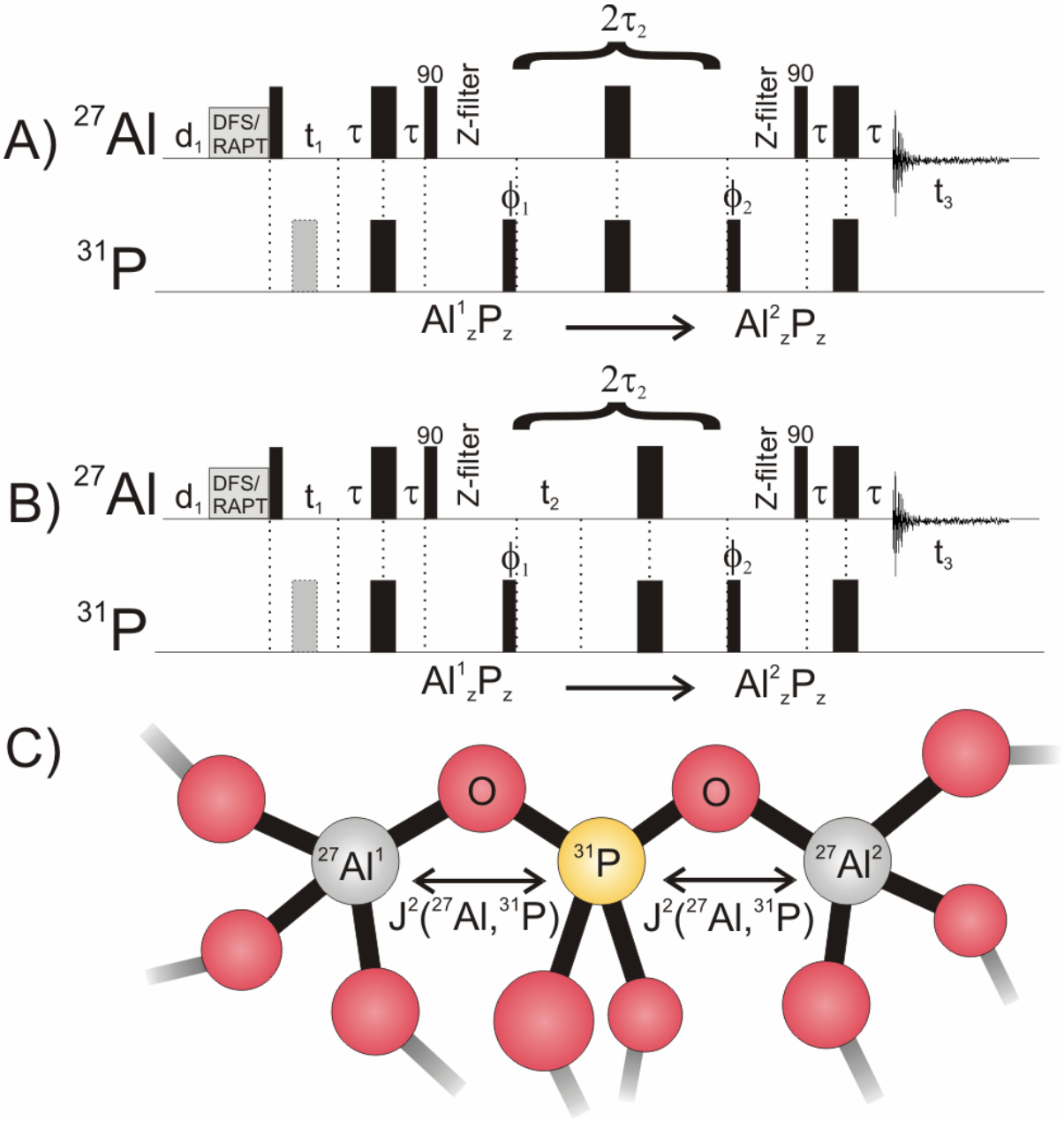
A)
27Al
d1
DFS/ RAPT
t1
τ
τ
90
Z-filter
2τ2
Z-filter
90
τ
τ
t3
ϕ1
ϕ2
31P
Al1zPz
Al2zPz
B)
27Al
d1
DFS/ RAPT
t1
τ
τ
90
Z-filter
t2
2τ2
Z-filter
90
τ
τ
t3
ϕ1
ϕ2
31P
Al1zPz
Al2zPz
C)
O
O
27Al1
31P
27Al2
J2(27Al,31P)
J2(27Al,31P)

Figure 2

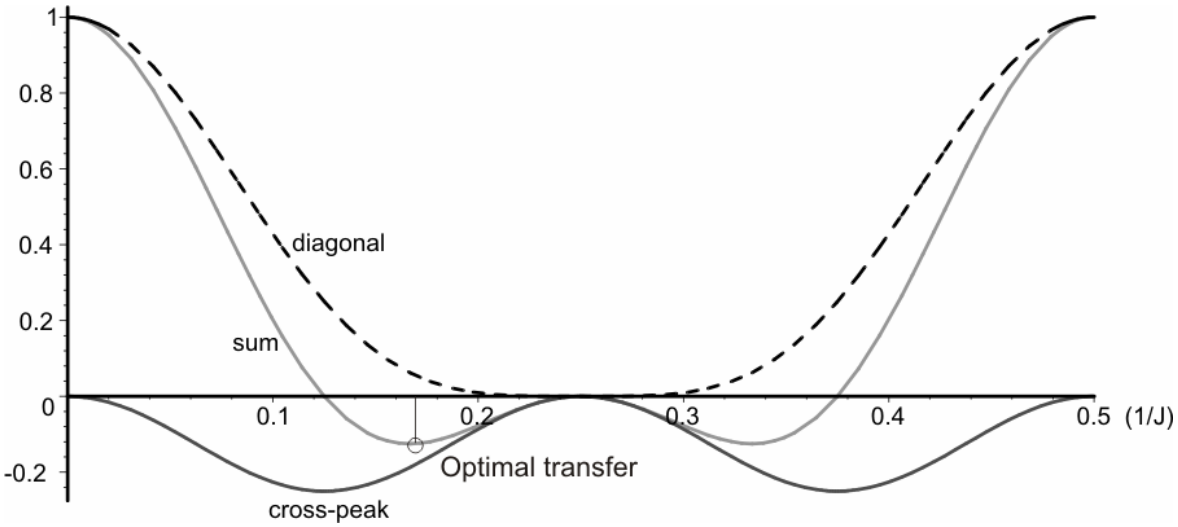
1
0.8
0.6
0.4
0.2
0
-0.2
diagonal
sum
0.1
0.2
0.3
0.4
0.5
(1/J)
Optimal transfer
cross-peak

Figure 3

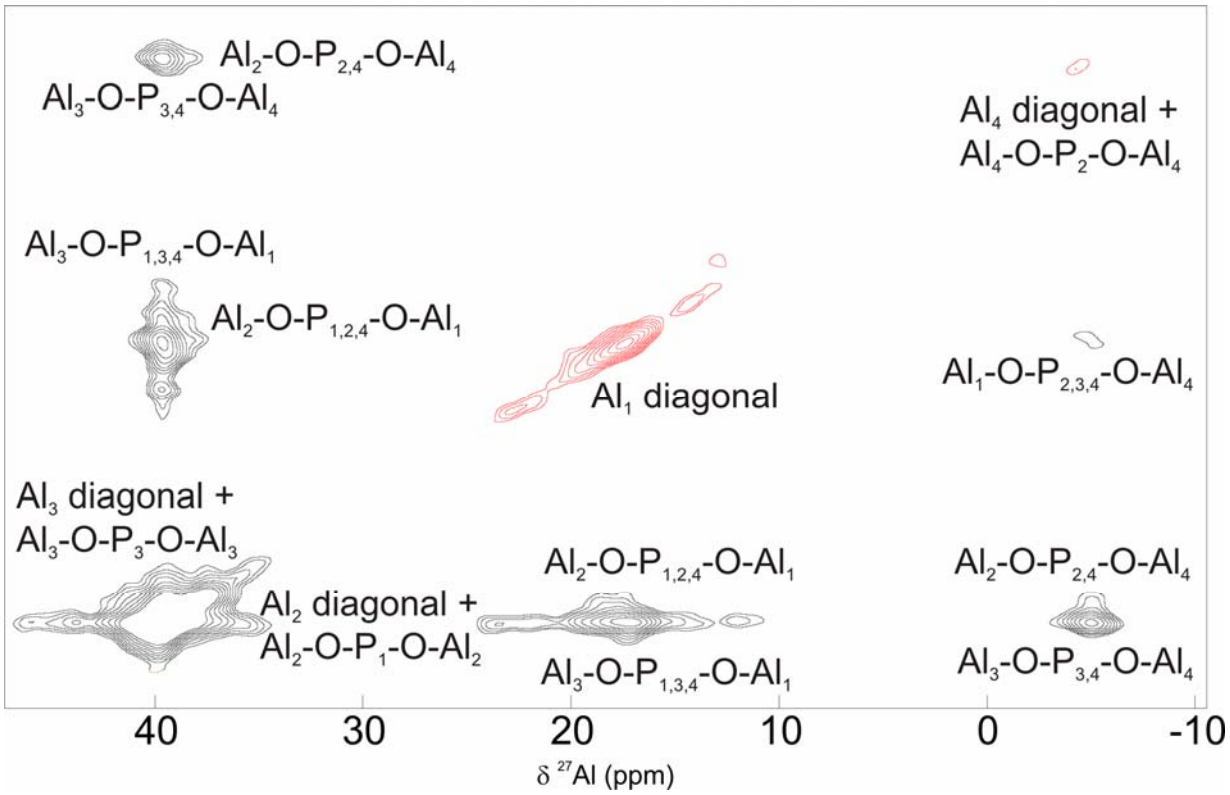
Al2-O-P2,4-O-Al4
Al3-O-P3,4-O-Al4
Al4 diagonal +
Al4-O-P2-O-Al4
Al3-O-P1,3,4-O-Al1
Al2-O-P1,2,4-O-Al1
Al1 diagonal
Al1-O-P2,3,4-O-Al4
Al3 diagonal +
Al3-O-P3-O-Al3
Al2 diagonal +
Al2-O-P1-O-Al2
Al2-O-P1,2,4-O-Al1
Al3-O-P1,3,4-O-Al1
Al2-O-P2,4-O-Al4
Al3-O-P3,4-O-Al4
40
30
20
10
0
-10
δ 27Al (ppm)

Figure 4

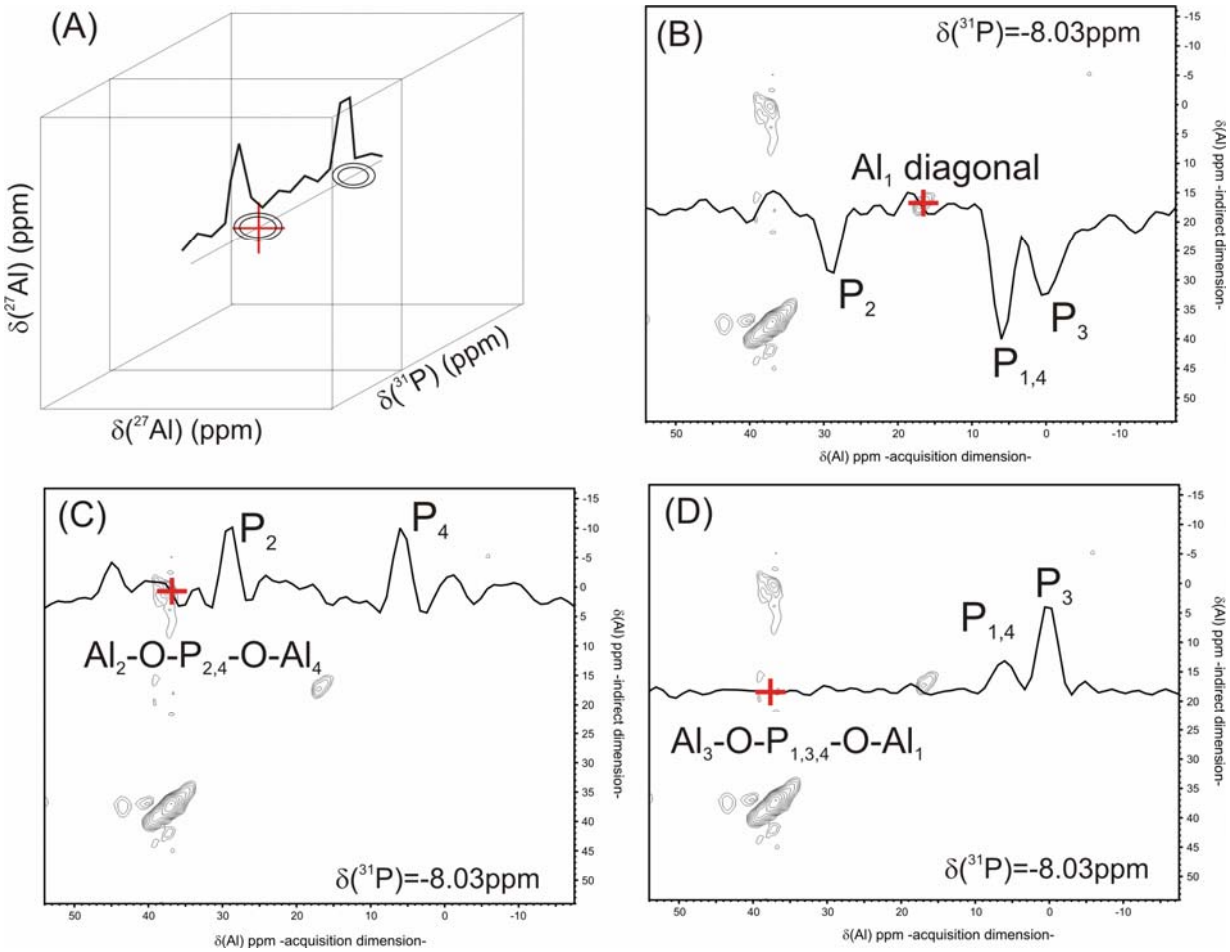


Figure 5

**Table 1** Al,P connectivity table for $AlPO_4$-14, as established in refs. *(7, 8)*.

| | $P_1$ | $P_2$ | $P_3$ | $P_4$ |
|---|---|---|---|---|
| $Al_1$ | 1 | 1 | 1 | 1 |
| $Al_2$ | 2 | 1 | 0 | 1 |
| $Al_3$ | 1 | 0 | 2 | 1 |
| $Al_4$ | 0 | 2 | 1 | 1 |

Michael Deschamps is a Maître de Conférences at the University of Orléans in France. He did his undergraduate work at the Ecole Normale Supérieure in Paris, where he was trained in NMR during his Ph.D. under the supervision of Prof. Geoffrey Bodenhausen. After a post-doctoral EMBO fellowship at the University of Oxford, where he worked with Prof. Iain Campbell and Dr. Jonathan Boyd, he joined the University of Orléans, working on solid-state NMR in the Centre de Recherche sur les Matériaux à Haute Température (CRMHT).

Dominique Massiot is a CNRS Directeur de Recherche at the CRMHT in Orléans. He did his Ph.D. in Geochemistry at the Paris VII University in 1983, and has been working ever since at the CRMHT using solid-state and high temperature NMR to tackle a wide variety of problems in inorganic chemistry. He is the author of “dmfit”, a widely used software for the interpretation of complex solid-state NMR spectra.